Editors' Suggestion

Large-Momentum-Transfer Atom Interferometers with μrad-Accuracy Using Bragg Diffraction

J.-N. Kirsten-Siemß,[1,2,*] F. Fitzek,[1,2] C. Schubert,[2,3] E. M. Rasel,[2] N. Gaaloul,[2] and K. Hammerer[1,†]
[1]Leibniz Universität Hannover, Institut für Theoretische Physik, Appelstraße 2, D-30167 Hannover, Germany
[2]Leibniz Universität Hannover, Institut für Quantenoptik, Welfengarten 1, D-30167 Hannover, Germany
[3]Deutsches Zentrum für Luft- und Raumfahrt e.V. (DLR), Institut für Satellitengeodäsie und Inertialsensorik, Callinstraße 30b, D-30167 Hannover, Germany

(Received 13 August 2022; revised 20 February 2023; accepted 25 May 2023; published 19 July 2023)

Large-momentum-transfer (LMT) atom interferometers using elastic Bragg scattering on light waves are among the most precise quantum sensors to date. To advance their accuracy from the mrad to the μrad regime, it is necessary to understand the rich phenomenology of the Bragg interferometer, which differs significantly from that of a standard two-mode interferometer. We develop an analytic model for the interferometer signal and demonstrate its accuracy using comprehensive numerical simulations. Our analytic treatment allows the determination of the atomic projection noise limit of a LMT Bragg interferometer and provides the means to saturate this limit. It affords accurate knowledge of the systematic phase errors as well as their suppression by 2 orders of magnitude down to a few μrad using appropriate light-pulse parameters.

DOI: 10.1103/PhysRevLett.131.033602

Atom interferometry enables the most precise determination of the fine-structure constant [1,2] and the most accurate quantum test of the universality of free fall [3]. Allowing absolute measurements of inertial forces [4] with high accuracy and precision, atom interferometers are ideally suited for real-world applications [5] like gravimetry [6,7], gravity cartography [8], and inertial navigation [9,10]. Notably, they recently enabled the observation of the gravitational Aharonov-Bohm effect [11]. Large-momentum-transfer (LMT) beam splitting is a key technology for quantum sensors with unprecedented precision, which may detect gravitational wave signatures and ultralight dark matter [12–17]. Using different beam-splitting techniques to increase the interferometer sensitivity, several LMT implementations demonstrated record-breaking spatial separations of coherent superpositions of matter waves [18–21]. To date, all LMT atom interferometers demonstrating metrological gain [1,3,11,22] use elastic Bragg scattering of atoms from time-dependent optical lattice potentials [23,24]. Compared to a two-mode interferometer, higher-order Bragg processes feature undesired diffraction orders [25,26] [see Fig. 1(a)], causing systematic uncertainties on the mrad level referred to as the diffraction phase [4,19,27–29]. Yet, a comprehensive analytical model of Bragg interferometers is still missing.

Here, we present such a model by taking into account the multiport and multipath physics of Bragg diffraction. We apply it to the popular Mach-Zehnder (MZ) geometry and demonstrate a straightforward way to suppress the diffraction phase via a suitable choice of pulse parameters. Figure 1(b) illustrates that a tailored combination of laser intensity and duration of the mirror pulse prevents the dominant parasitic paths from closing interferometers. We show that by largely suppressing the parasitic interferences, the physics of the diffraction phase simplifies dramatically to a mere offset that can be readily determined. This allows us to reduce the systematic error below the mrad level, when considering high-order Bragg beam splitters [25,26] with less than 10% diffraction losses. We verify the accuracy of our model by comparison to simulations of the MZ interferometer in numerical experiments.

Beyond systematic effects, parasitic paths and undetected open ports affect the statistical properties of the measurement. The statistical uncertainty is defined by the

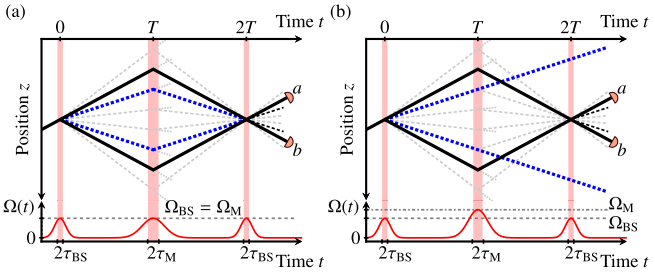

FIG. 1. Space-time diagrams of MZ interferometers. Top row: nth-order Bragg beam splitters (BS) populating the main trajectories (solid black lines), open ports, and parasitic paths (dashed lines; the dominant ones for $n = 5$ are thick blue lines), all affecting the MZ signal recorded in ports a, b. Trajectories are shown in the optical lattice frame. Bottom row: Gaussian pulses $\Omega(t)$ with pulse widths $\tau_{BS,M}$ spaced by time T. While in panel (a) we choose identical peak Rabi frequencies Ω (which we refer to as MZ type A), panel (b) illustrates deflection of dominant spurious paths with a tailored choice for Ω_M, τ_M (MZ type B).

(quantum) Cramér-Rao bounds [(Q)CRB] [30], which modify the standard quantum limit and are yet to be determined for Bragg interferometers. We show that the (Q)CRB exhibit a nontrivial dependence on the unavoidable diffraction losses. Moreover, we demonstrate that the phase estimation strategies presented here allow saturation of these fundamental bounds. Our study of the atomic projection noise establishes important design criteria for the operation of Bragg interferometers at or below the standard quantum limit [31–34].

Analytical model of Bragg MZ interferometers.—In Bragg diffraction, the intensity and relative frequencies, $2\delta \equiv \omega_1 - \omega_2$, of two counterpropagating light fields are adjusted to transfer a multiple of twice the photon recoil $2n\hbar k$ via pulsed optical lattices, $V(t) = 2\hbar\Omega(t)\cos[k\hat{z} - \delta t + \phi_{\mathrm{L}}(t)]$. Additionally, the phase of the light field $\phi_{\mathrm{L}}(t)$ is imprinted on the atomic wave function. The integer n denotes the Bragg order, and we focus on smooth Gaussian two-photon Rabi frequencies, $\Omega(t) = \Omega e^{-t^2/2\tau^2}$, which reduce the coupling to undesired diffraction orders [25]. Different peak Rabi frequencies Ω and pulse widths τ lead to beam-splitter and mirror operations if they fulfill the respective condition on the pulse area [25,26]. This freedom gives the possibility to balance between losses into unwanted momentum states and lower diffraction efficiencies due to the Doppler effect [26,35] which are dominating at short and long pulses, respectively.

We characterize the two beam splitters and the mirror that form the MZ interferometer via Ω_{BS}, τ_{BS} and $\Omega_{\mathrm{M}}, \tau_{\mathrm{M}}$, respectively. We extend our previous treatment of single pulses in Ref. [26] to include the dominant parasitic Bragg orders; see Supplemental Material (SM) [36]. By combining transfer matrices that account for diffraction and free propagation, we obtain a scattering matrix of the MZ, $\mathcal{S}_{\mathrm{MZ}}(\phi, T, \Omega_{\mathrm{BS}}, \tau_{\mathrm{BS}}, \Omega_{\mathrm{M}}, \tau_{\mathrm{M}})$, which depends on the metrological phase ϕ in addition to the pulse parameters. We describe the incoming atoms by a Gaussian wave packet, $|\psi^{\mathrm{in}}(\sigma_p)\rangle$, centered around $-n\hbar k$ and featuring a momentum width well below the photon recoil, $\sigma_p \ll \hbar k$, considering ultracold sources [46,47]. Thus, the relative atom number signals in ports a and b in Fig. 1, $P_{a(b)}(\phi) = N_{a(b)}(\phi)/[N_a(\phi) - N_b(\phi)]$, can be calculated via the output state $|\psi^{\mathrm{out}}(\phi, T, \Omega_{\mathrm{BS}}, \tau_{\mathrm{BS}}, \Omega_{\mathrm{M}}, \tau_{\mathrm{M}}, \sigma_p)\rangle = \mathcal{S}_{\mathrm{MZ}}|\psi^{\mathrm{in}}(\sigma_p)\rangle$; see SM [36].

Phase estimation usually requires fitting a model $P_a(\phi)$ to the signal $P_a^{\mathrm{meas}}(\phi)$ recorded by scanning ϕ, e.g., via the phase ϕ_{L}. The use of relative populations suppresses statistical fluctuations in the initial atom number N_{atoms}. Since the estimate relies on the inversion $\phi^{\mathrm{est}} = P_a^{-1}(P_a^{\mathrm{meas}})$, the quality of the model crucially affects the systematic accuracy and the statistical sensitivity of the phase measurement.

Interferometer including parasitic paths.—Depending on the pulse parameters, interferometers realized through higher-order Bragg pulses exhibit parasitic interferometers and open ports to varying degrees; see Fig. 1(a). Their effect on the interferometer signal can be substantial [48–50]. Our analytical model for $|\psi_{\mathrm{out}}\rangle$ reflects this in a signal for the relative atom number measurement, which takes the form of an infinite Fourier series,

$$P_a^{\mathrm{exact}}(\phi) = P_0 + \sum_{j=1}^{\infty} A_j \cos(j\phi + \varphi_j), \tag{1}$$

whose coefficients P_0, A_j, φ_j derive from $|\psi_{\mathrm{out}}\rangle$; see SM [36]. We contrast this with the standard result for an idealized two-mode MZ interferometer of order n, $P_{a(b)}^{\mathrm{ideal}}(\phi) = P_0 \pm A\cos n\phi$.

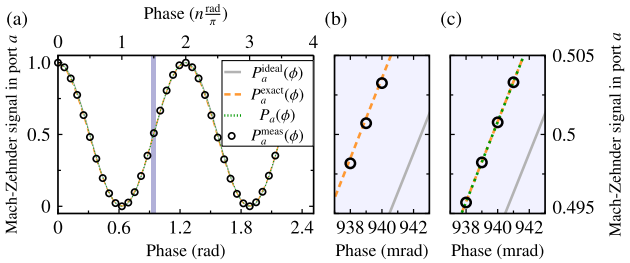

FIG. 2. MZ signal phase scan in port a. (a),(b) Comparison of numerical simulations $P_a^{\mathrm{meas}}(\phi)$ (symbols) with analytical predictions of Eqs. (1) (orange dashed line) and (2) (green dotted line) and with the sinusoidal signal, $P_{\mathrm{a}}^{\mathrm{ideal}}(\phi) = (1 + \cos n\phi)/2$ (gray solid line). The parameters $\Omega, \tau_{\mathrm{BS}}, \tau_{\mathrm{M}} = 28.5\omega_{\mathrm{r}}, 0.309\omega_{\mathrm{r}}^{-1}, 0.681\omega_{\mathrm{r}}^{-1}$ cause approximately 1.4% beam-splitter losses and amplify signal distortions. Here, $\omega_{\mathrm{r}} = \hbar k^2/2m$ is the recoil frequency of an atom with mass m, and we scan the relative phase $\phi_{\mathrm{L}}(t) = \phi_{\mathrm{L}}$ of the final beam splitter. Zooms in panels (b) and (c) reveal a mrad shift relative to $P_{\mathrm{a}}^{\mathrm{ideal}}(\phi)$. Using adapted mirror parameters $\Omega_{\mathrm{M}}, \tau_{\mathrm{M}} = 31.8\omega_{\mathrm{r}}, 0.463\omega_{\mathrm{r}}^{-1}$ as in Fig. 1(b), panel (c) confirms agreement between the numerics and both analytical models at the mrad level, which we quantify below.

Including dominant parasitic paths for $n = 5$ in Figs. 2(a) and 2(b), we demonstrate good agreement between Eq. (1) and numerical simulations. The latter are based on a one-dimensional description of the complete matter-wave interferometer in position space as per Ref. [51], accounting for all diffraction orders. We scan the phase via the final beam splitter, selecting different values $\phi_{\mathrm{L}} = \phi_{\mathrm{L}}(t)$ for each data point, and we set $\Omega = \Omega_{\mathrm{BS}} = \Omega_{\mathrm{M}}$. In the following, we refer to this configuration shown in Fig. 1(a) as MZ type A. Suitable pulse widths $\tau_{\mathrm{BS}}, \tau_{\mathrm{M}}$ satisfy the pulse area conditions [25,26] and provide high diffraction efficiencies, yielding a loss of 1.4% after the first beam splitter. Yet, Fig. 2(b) shows that the ideal sinusoidal signal is shifted by several mrad, making it an inaccurate description.

References [48–50] provide evidence of undesired additional Fourier components whose origin can be understood as follows: (i) Multiport Bragg beam splitters render the

combined atom number in the detected ports phase dependent, $N_a(\phi)+N_b(\phi)=N_{\text{atoms}}-N_{\text{open}}(\phi)$. Here, $N_{\text{open}}(\phi)$ denotes the population of all undetected (open) output ports; see Fig. 1. The relative atom numbers, $N_{a(b)}(\phi)/[N_{\text{atoms}}-N_{\text{open}}(\phi)]$, are thus ratios of ϕ-dependent functions and generally contain Fourier components of arbitrary order. In contrast, considering idealized two-mode interferometers, we simply obtain $N_{\text{atoms}}=N_a(\phi)+N_b(\phi)$. (ii) Moreover, the absolute atom numbers $N_{a(b)}(\phi)$ contain additional parasitic interference terms (cf. Refs. [48,50]) due to the spatial overlap of undesired diffraction orders with the main interferometry arms at $t=2T$, as shown in Fig. 1(a). In particular, asymmetric spurious interferometers make the coefficients in Eq. (1) depend on the interrogation time T, as observed in Refs. [48,49]. Notwithstanding its correctness, in experiments, it will be challenging to use the waveform in Eq. (1) for phase estimation due to the large number of parameters involved and the limited control over them.

Interferometer with suppressed parasitic paths.—Figure 1(b) illustrates the suppression of spurious interference terms using the MZ mirror. In this configuration, which we will call MZ type B, the central pulse can efficiently deflect the dominant spurious trajectories for all Bragg orders $n\geq 3$. In addition to stating the corresponding parameters $\Omega_{\text{M}}, \tau_{\text{M}}$ for $n=5$, we explain the exception of the $n=2$ MZ geometry in the SM [36]. It is straightforward to suppress parasitic interferences in our analytical model and consider only the effects of the open ports [point (i) above]. Doing so simplifies the MZ signal to

$$P_{a(b)}(\phi)=P_0\pm\sum_{j=1}^{3}A_j\sin\left[j\left(n\phi+\gamma+\frac{\pi}{2}\right)\right]+\mathcal{O}[\gamma^3], \tag{2}$$

where $P_b(\phi)$ is shifted by π as expected; see SM [36]. Compared to Eq. (1), this expression contains only the harmonics of a single Fourier component $n\phi$ and a phase shift γ common to all harmonics. In fact, γ is a small parameter closely related to the losses to undesired diffraction orders during beam splitting [26] and therefore can be calculated given the parameters $\Omega_{\text{BS}}, \tau_{\text{BS}}$; see SM [36]. Considering a MZ interferometer with suppressed parasitic paths as in Fig. 1(b), Fig. 2(c) shows excellent agreement at the mrad level between the complex signal in Eq. (1) and the much simpler formula in Eq. (2) with the numerical simulations.

Diffraction phase.—We further quantify the accuracy of phase estimates $\phi^{\text{est}}=P_a^{-1}(P_a^{\text{meas}})$ that are applied to numerical simulations of MZ interferometers as in Fig. 1 and based on Eq. (2). The systematic deviation between ϕ^{est} and the true value ϕ is called the diffraction phase [28,49],

$$\delta\phi=P_a^{-1}(P_a^{\text{meas}})-\phi=P_a^{-1}(P_a^{\text{meas}})|_{\gamma=0}-\phi-\frac{\gamma}{n}. \tag{3}$$

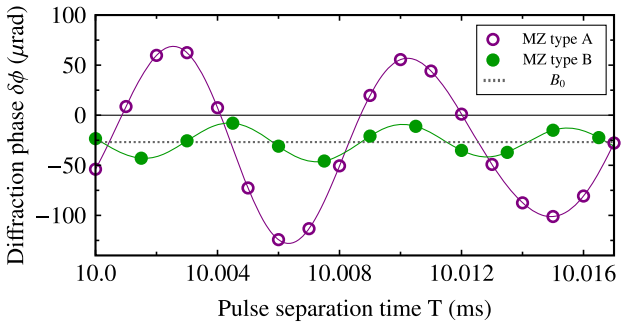

FIG. 3. Phase estimation error. Diffraction phases $\delta\phi$ in Eq. (3) evaluated for numerically simulated MZ interferometers with different separation times T. Operation at the so-called "magic" Bragg beam-splitter duration for $n=5$ (see main text) reduces oscillation amplitudes for both MZ configurations to less than or equal to 200 μrad due to small diffraction losses of approximately 0.18% (cf. Refs. [48,49]). Open circles (MZ type A) assume parameters $\Omega, \tau_{\text{BS}}, \tau_{\text{M}}=30.75\omega_{\text{r}}, 0.218\omega_{\text{r}}^{-1}, 0.519\omega_{\text{r}}^{-1}$, while the adapted Bragg mirror $\Omega_{\text{M}}, \tau_{\text{M}}=31.8\omega_{\text{r}}, 0.463\omega_{\text{r}}^{-1}$ (closed circles, MZ type B) further suppresses the peak-to-peak value by a factor of 5 to less than 40 μrad. Fits to the data (solid lines) show identical offsets $B_0\approx -27$ μrad (dotted line) for both sets.

In the second equality, we used the fact that in Eq. (2) γ is a shift common to all Fourier components. Moreover, γ can be inferred quite accurately for given Ω_{BS}, τ_{BS}; see SM [36]. Thus, the error of $P_a(\phi)$ with respect to the remaining phase, $P_a^{-1}(P_a^{\text{meas}})|_{\gamma=0}$, determines the systematic uncertainty. Additionally, scaling with $n\phi$ in Eq. (2) leads to a linear suppression of $\delta\phi$ with the Bragg order n; cf. Ref. [28].

After fitting $P_a(\phi)$ in Eq. (2) to numerical signals, P_a^{meas}, of $n=5$ MZ interferometers of types A and B with different separation times $T\in[10, 10.017]$ ms, we evaluate $\delta\phi$ in Fig. 3. Spurious interference terms cause oscillations with T at frequencies $(5\pm 1)\,8\omega_{\text{r}}$ proportional to the recoil frequency $\omega_{\text{r}}=\hbar k^2/2m$ (cf. Refs. [48,49]) of an atomic mass m. Despite minimizing the beam-splitter losses to approximately 0.18%, we observe oscillations at the μrad level, which result from the kinetic energy difference between main interferometer arms and spurious paths; cf. Refs. [48,49]. We use beam-splitter parameters that Parker *et al.* refer to as magic Bragg duration for $n=5$ as they effectively reduce similar oscillations in the conjugated Ramsey-Bordé interferometer in Ref. [49]. Fitting $f(T)=B_0+B_1\cos(4\,8\omega_{\text{r}}T+\nu_1)+B_2\cos(6\,8\omega_{\text{r}}T+\nu_2)$ to the data in Fig. 3 reveals the same offset $B_0\approx -27$ μrad without (MZ type A) and with (MZ type B) suppression of parasitic paths. Thus, the inclusion of $\gamma/n\approx 280$ μrad in Eq. (3) accounts for most of the T-independent shift. In contrast, the adapted mirror suppresses the peak-to-peak (PP) value $\text{PP}:=|\max_{\forall T}f(T)-\min_{\forall T}f(T)|$ by about 80% to less than 40 μrad. This is significant because the net diffraction phase shift can be of similar magnitude due to insufficient

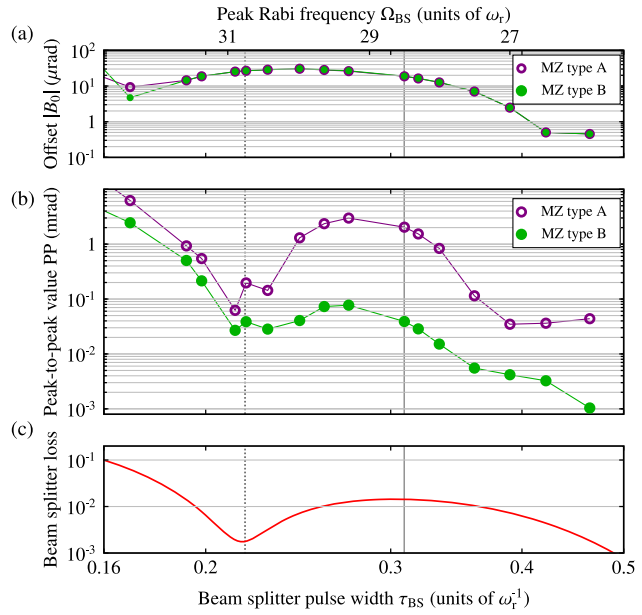

FIG. 4. Diffraction phase suppression. (a,b) Data points characterizing oscillations in $\delta\phi$ for MZ configurations A (open symbols) and B (closed symbols) as in Fig. 3, but for a range of pulse parameters; see SM [36]. Lines between symbols serve as a guide for the eye. (a) Offsets $|B_0| \leq 30$ μrad (symbols), which are largely identical for both MZ types. Panel (b) shows that in case B, peak-to-peak (PP) values are mostly below 1 mrad and less than 10 μrad for sufficiently long pulse durations. (c) Numerically determined diffraction loss of a fifth-order Bragg beam splitter (coupling $|\pm 5\hbar k\rangle$). Parameters used in Fig. 2 (Fig. 3) correspond to the visible local maximum (minimum) denoted by the solid (dotted) vertical line.

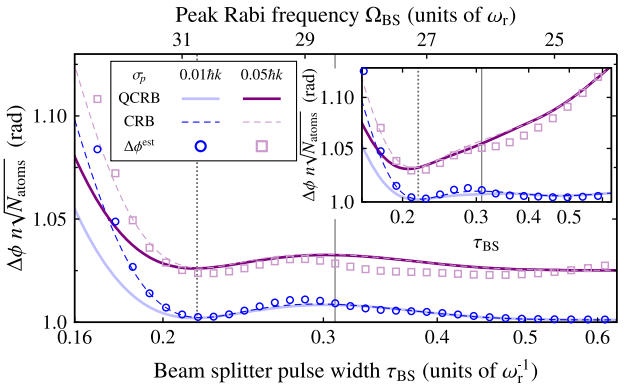

FIG. 5. Sensitivity bounds for uncorrelated particles. Cramér-Rao bound (dashed lines) and quantum Cramér-Rao bound (solid lines) for $n = 5$ scanning Ω_{BS}, τ_{BS} with $T = 10$ ms. Results are scaled to the projection noise of an ideal two-mode MZ, $n\sqrt{N_{atoms}}$. Symbols represent the statistical uncertainty $\Delta\phi^{est}(\phi)$ of phase estimates based on Eq. (2) applied to numerical MZ signals. Both CRB and $\Delta\phi^{est}$ are obtained at midfringe ($\phi = \frac{3\pi}{2}\frac{1}{5}$). The adapted Bragg mirror $\Omega_M, \tau_M = 31.8\omega_r, 0.463\omega_r^{-1}$ (case B) suppresses parasitic interference and, compared to case A in the inset, is less susceptible to the finite velocity spread of the wave packet $\sigma_p = 0.01\hbar k$ ($0.05\hbar k$) in blue (purple) at longer pulse durations. The dotted (solid) vertical line again corresponds to the local minimum (maximum) in the losses in Fig. 4(c).

control over the separation time T at the μs level or because of aliasing effects when T is sampled; cf. Ref. [49].

In Figs. 4(a) and 4(b), we compare offsets $|B_0|$ and PP between both Bragg mirror configurations for a parameter range Ω_{BS}, τ_{BS} ensuring less than 10% beam-splitter losses. Figure 4(a) confirms that accounting for γ in Eq. (3) reduces the remaining T-independent contribution to $\delta\phi$ to at most a few tenths of μrad independent of the mirror. In contrast, Fig. 4(b) shows that the adapted mirror effectively suppresses the oscillations of $\delta\phi$. For relatively strong couplings to undesired diffraction orders, we observe PP values that are comparable to γ/n and on the order of several mrad; see SM [36]. Figure 4(c) shows the close relation between $\delta\phi$ and the beam-splitter losses. Notably, the local minimum indicates the aforementioned magic Bragg duration for $n = 5$, but in fact, such minima exist for all orders $n > 1$ and are a feature predicted by Landau-Zener theory [26].

In summary, using Eq. (2) (including γ) and adapting the central MZ pulse to suppress parasitic interference reduces the diffraction phase below 1 mrad for most parameters Ω_{BS}, τ_{BS}. Assuming sufficiently long beam-splitter durations, we predict only a few μrad. In contrast, not including the diffraction phase offset γ in Eq. (2) and not suppressing parasitic interference would increase the systematic error to more than 0.5 mrad. This represents an improvement of 2 orders of magnitude, limited only by higher-order contributions in γ and a finite efficiency in suppressing the spurious paths.

Phase sensitivity.—Finally, we discuss the statistical uncertainty of the estimate $\phi^{est} = P_a^{-1}(P_a^{meas})$ based on Eq. (2). We note that the projection noise $\Delta\phi^{est}(\phi) \approx \sqrt{[P_a(\phi)(1-P_a(\phi))]/[N_a(\phi)+N_b(\phi)]}\{1/[|\partial_\phi P_a(\phi)_\phi|]\}$ (see SM [36]) can be quite different from that of a two-mode MZ interferometer, which evaluates to $\Delta\phi^{est} = \{[\sqrt{P_0(1-P_0)}]/[nA\sqrt{N_{atoms}}]\}$ at midfringe $P_a(\phi) = 0.5$. We compare the phase sensitivity with the QCRB and the CRB both derived from $|\psi^{out}\rangle$; see SM [36]. While the CRB considers relative atom number measurements in ports a and b, the QCRB bounds the projection noise for arbitrary measurements performed on all output ports of the final pulse.

Assuming the same pulse parameters as before, Fig. 5 (case A in inset) shows that the projection noise limit for a Bragg interferometer lies a few percent above the CRB of an ideal two-mode interferometer ($P_0 = A = 1/2$): $\Delta\phi^{est} = (n\sqrt{N_{atoms}})^{-1}$. Moreover, we find good agreement between the analytical CRB and QCRB and the uncertainty $\Delta\phi^{est}$ of Eq. (2) applied to the numerical data. The visible

deviations are at the expected level given our perturbative treatment of finite velocity effects and beam-splitter losses; see SM [36]. Sensitivity is lost at shorter pulses due to increasing diffraction losses; see Fig. 4(c). Towards longer pulses, the velocity selectivity of the Bragg process leads to atom loss and an increase of the CRB, especially for wave packets with larger momentum spreads σ_p; cf. Ref. [35]. We note that in case B, the velocity selectivity of the mirror is reduced because of the relatively short pulse duration chosen to deflect the dominant parasitic paths; see SM [36]. Since the diffraction losses primarily populate parasitic interferometers with reduced scale factors less than n, the resulting decrease in the space-time area worsens the statistical uncertainty of the phase measurement. Therefore, despite the intentional deflection of atoms from the interferometer in scenario B [cf. Fig. 1(b)], we see no difference in performance between the two configurations. Operation at the local minimum of the beam-splitter losses in Fig. 4(c) ensures the best sensitivity. This sets the fundamental projection noise limit of a Bragg atom interferometer.

Conclusions.—Our analytical model provides a thorough understanding of the systematic and statistical uncertainties of LMT Bragg atom interferometers. Hence, it yields design criteria for reaching the fundamental sensitivity bounds of these devices and paves the way towards accuracies in the μrad range when using ultracold atomic sources [46,47]. Operation of LMT interferometers at or near the quantum projection noise limit is a critical requirement if they are to be combined with entangled sources [33,34]. The methods developed here are applicable to other configurations such as the conjugated Ramsey-Bordé interferometer (cf. Ref. [1]) or double Bragg diffraction [52–54]. Our work contributes to the development of high-precision quantum sensors for fundamental tests and to atom interferometers fulfilling the size, weight, and power (SWAP) requirements of modern real-world applications [4,29], especially in combination with resonator-enhanced light fields [55,56].

The results presented here were partially achieved by computations carried out on the cluster system at the Leibniz University of Hannover, Germany. We thank A. Gauguet and S. Loriani for helpful comments on the manuscript. This work was funded by the Deutsche Forschungsgemeinschaft (German Research Foundation) under Germany's Excellence Strategy (EXC-2123 QuantumFrontiers Grant No. 390837967), through CRC 1227 (DQ-mat) within Projects No. A05, No. B07, as well as No. B09, and QuantERA Project No. 499225223 (SQUEIS), and the German Space Agency (DLR) with funds provided by the German Federal Ministry of Economic Affairs and Energy (BMWi) from an enactment of the German Bundestag under Grant No. DLR 50WM1952 (QUANTUS-V-Fallturm), 50WP1700 (BECCAL), 50NA1957 (QGYRO), 50NA2106 (QGYRO+), 50WM2250A (QUANTUS-plus), 50WM2245A (CAL-II), 50WM2263A (CARIOQA-GE), 50WM2253A (AI-quadrat). We furthermore acknowledge financial support from "Niedersächsisches Vorab" through "Förderung von Wissenschaft und Technik in Forschung und Lehre" for the initial funding of research in the new DLR-SI Institute.

*jan-niclas.siemss@itp.uni-hannover.de
†klemens.hammerer@itp.uni-hannover.de

[1] R. H. Parker, C. Yu, W. Zhong, B. Estey, and H. Müller, Measurement of the fine-structure constant as a test of the standard model, Science **360**, 191 (2018).
[2] L. Morel, Z. Yao, P. Cladé, and S. Guellati-Khélifa, Determination of the fine-structure constant with an accuracy of 81 parts per trillion, Nature (London) **588**, 61 (2020).
[3] P. Asenbaum, C. Overstreet, M. Kim, J. Curti, and M. A. Kasevich, Atom-Interferometric Test of the Equivalence Principle at the 10^{-12} Level, Phys. Rev. Lett. **125**, 191101 (2020).
[4] R. Geiger, A. Landragin, S. Merlet, and F. Pereira Dos Santos, High-accuracy inertial measurements with cold-atom sensors, AVS Quantum Sci. **2**, 024702 (2020).
[5] K. Bongs, M. Holynski, J. Vovrosh, P. Bouyer, G. Condon, E. Rasel, C. Schubert, W. P. Schleich, and A. Roura, Taking atom interferometric quantum sensors from the laboratory to real-world applications, Nat. Rev. Phys. **1**, 731 (2019).
[6] V. Ménoret, P. Vermeulen, N. Le Moigne, S. Bonvalot, P. Bouyer, A. Landragin, and B. Desruelle, Gravity measurements below $10^{-9}g$ with a transportable absolute quantum gravimeter, Sci. Rep. **8**, 12300 (2018).
[7] X. Wu, Z. Pagel, B. S. Malek, T. H. Nguyen, F. Zi, D. S. Scheirer, and H. Müller, Gravity surveys using a mobile atom interferometer, Sci. Adv. **5**, eaax0800 (2019).
[8] B. Stray *et al.*, Quantum sensing for gravity cartography, Nature (London) **602**, 590 (2022).
[9] R. Geiger, V. Ménoret, G. Stern, N. Zahzam, P. Cheinet, B. Battelier, A. Villing, F. Moron, M. Lours, Y. Bidel, A. Bresson, A. Landragin, and P. Bouyer, Detecting inertial effects with airborne matter-wave interferometry, Nat. Commun. **2**, 474 (2011).
[10] P. Cheiney, L. Fouché, S. Templier, F. Napolitano, B. Battelier, P. Bouyer, and B. Barrett, Navigation-Compatible Hybrid Quantum Accelerometer Using a Kalman Filter, Phys. Rev. Appl. **10**, 034030 (2018).
[11] C. Overstreet, P. Asenbaum, J. Curti, M. Kim, and M. A. Kasevich, Observation of a gravitational Aharonov-Bohm effect, Science **375**, 226 (2022).
[12] P. W. Graham, J. M. Hogan, M. A. Kasevich, and S. Rajendran, New Method for Gravitational Wave Detection with Atomic Sensors, Phys. Rev. Lett. **110**, 171102 (2013).
[13] B. Canuel, A. Bertoldi, L. Amand *et al.*, Exploring gravity with the MIGA large scale atom interferometer, Sci. Rep. **8**, 14064 (2018).
[14] B. Canuel *et al.*, ELGAR—A European laboratory for gravitation and atom-interferometric research, Classical Quantum Gravity **37**, 225017 (2020).

[15] M.-S. Zhan *et al.*, ZAIGA: Zhaoshan long-baseline atom interferometer gravitation antenna, Int. J. Mod. Phys. D **29**, 1940005 (2020).

[16] L. Badurina *et al.*, AION: An atom interferometer observatory and network, J. Cosmol. Astropart. Phys. 05 (2020) 011.

[17] M. Abe *et al.*, Matter-wave atomic gradiometer interferometric sensor (MAGIS-100), Quantum Sci. Technol. **6**, 044003 (2021).

[18] S.-w. Chiow, T. Kovachy, H.-C. Chien, and M. A. Kasevich, 102$\hbar$ k Large Area Atom Interferometers, Phys. Rev. Lett. **107**, 130403 (2011).

[19] B. Plotkin-Swing, D. Gochnauer, K. E. McAlpine, E. S. Cooper, A. O. Jamison, and S. Gupta, Three-Path Atom Interferometry with Large Momentum Separation, Phys. Rev. Lett. **121**, 133201 (2018).

[20] M. Gebbe, J.-N. Siemß, M. Gersemann, H. Müntinga, S. Herrmann, C. Lämmerzahl, H. Ahlers, N. Gaaloul, C. Schubert, K. Hammerer, S. Abend, and E. M. Rasel, Twin-lattice atom interferometry, Nat. Commun. **12**, 2544 (2021).

[21] T. Wilkason, M. Nantel, J. Rudolph, Y. Jiang, B. E. Garber, H. Swan, S. P. Carman, M. Abe, and J. M. Hogan, Atom Interferometry with Floquet Atom Optics, Phys. Rev. Lett. **129**, 183202 (2022).

[22] P. Asenbaum, C. Overstreet, T. Kovachy, D. D. Brown, J. M. Hogan, and M. A. Kasevich, Phase Shift in an Atom Interferometer due to Spacetime Curvature across its Wave Function, Phys. Rev. Lett. **118**, 183602 (2017).

[23] P. J. Martin, B. G. Oldaker, A. H. Miklich, and D. E. Pritchard, Bragg Scattering of Atoms from a Standing Light Wave, Phys. Rev. Lett. **60**, 515 (1988).

[24] D. M. Giltner, R. W. McGowan, and S. A. Lee, Theoretical and experimental study of the Bragg scattering of atoms from a standing light wave, Phys. Rev. A **52**, 3966 (1995).

[25] H. Müller, S.-w. Chiow, and S. Chu, Atom-wave diffraction between the Raman-Nath and the Bragg regime: Effective Rabi frequency, losses, and phase shifts, Phys. Rev. A **77**, 023609 (2008).

[26] J.-N. Siemß, F. Fitzek, S. Abend, E. M. Rasel, N. Gaaloul, and K. Hammerer, Analytic theory for Bragg atom interferometry based on the adiabatic theorem, Phys. Rev. A **102**, 033709 (2020).

[27] M. Büchner, R. Delhuille, A. Miffre, C. Robilliard, J. Vigué, and C. Champenois, Diffraction phases in atom interferometers, Phys. Rev. A **68**, 013607 (2003).

[28] B. Estey, C. Yu, H. Müller, P.-C. Kuan, and S.-Y. Lan, High-Resolution Atom Interferometers with Suppressed Diffraction Phases, Phys. Rev. Lett. **115**, 083002 (2015).

[29] F. A. Narducci, A. T. Black, and J. H. Burke, Advances toward fieldable atom interferometers, Adv. Phys. **7**, 1946426 (2022).

[30] C. W. Helstrom, Quantum detection and estimation theory, J. Stat. Phys. **1**, 231 (1969).

[31] L. Salvi, N. Poli, V. Vuletić, and G. M. Tino, Squeezing on Momentum States for Atom Interferometry, Phys. Rev. Lett. **120**, 033601 (2018).

[32] A. Shankar, L. Salvi, M. L. Chiofalo, N. Poli, and M. J. Holland, Squeezed state metrology with Bragg interferometers operating in a cavity, Quantum Sci. Technol. **4**, 045010 (2019).

[33] S. S. Szigeti, S. P. Nolan, J. D. Close, and S. A. Haine, High-Precision Quantum-Enhanced Gravimetry with a Bose-Einstein Condensate, Phys. Rev. Lett. **125**, 100402 (2020).

[34] R. Corgier, N. Gaaloul, A. Smerzi, and L. Pezzè, Delta-Kick Squeezing, Phys. Rev. Lett. **127**, 183401 (2021).

[35] S. S. Szigeti, J. E. Debs, J. J. Hope, N. P. Robins, and J. D. Close, Why momentum width matters for atom interferometry with Bragg pulses, New J. Phys. **14**, 023009 (2012).

[36] See Supplemental Material at http://link.aps.org/supplemental/10.1103/PhysRevLett.131.033602 for the definition of the scattering matrix formalism and for additional information about the Bragg diffraction pulse parameters used in this Letter. It includes Refs. [37–45].

[37] P. Storey and C. Cohen-Tannoudji, The Feynman path integral approach to atomic interferometry. A tutorial, J. Phys. II **4**, 1999 (1994).

[38] M. O. Scully and M. S. Zubairy, *Quantum Optics* (Cambridge University Press, Cambridge, England, 1997), 10.1017/CBO9780511813993.

[39] C. J. Bordé, Quantum theory of atom-wave beam splitters and application to multidimensional atomic gravito-inertial sensors, Gen. Relativ. Gravit. **36**, 475 (2004).

[40] P. Meystre, in *Atom Optics*, 3rd ed. (Springer, Germany, 2009), Chap. 4, pp. 57–68, https://link.springer.com/9780387952741.

[41] J. M. Hogan, D. M. S. Johnson, and M. A. Kasevich, in Atom Interferometry, *Proceedings of the International School of Physics "Enrico Fermi"*, edited by E. Arimondo, W. Ertmer, W. P. Schleich, and E. M. Rasel (Societ'a Italiana di Fisica and IOS Press, Amsterdam, 2009), pp. 411–447.

[42] S. A. Haine and M. T. Johnsson, Dynamic scheme for generating number squeezing in Bose-Einstein condensates through nonlinear interactions, Phys. Rev. A **80**, 023611 (2009).

[43] M. Kritsotakis, S. S. Szigeti, J. A. Dunningham, and S. A. Haine, Optimal matter-wave gravimetry, Phys. Rev. A **98**, 023629 (2018).

[44] L. Pezzè, A. Smerzi, M. K. Oberthaler, R. Schmied, and P. Treutlein, Quantum metrology with nonclassical states of atomic ensembles, Rev. Mod. Phys. **90**, 035005 (2018).

[45] D. Gochnauer, K. E. McAlpine, B. Plotkin-Swing, A. O. Jamison, and S. Gupta, Bloch-band picture for light-pulse atom diffraction and interferometry, Phys. Rev. A **100**, 043611 (2019).

[46] T. Kovachy, J. M. Hogan, A. Sugarbaker, S. M. Dickerson, C. A. Donnelly, C. Overstreet, and M. A. Kasevich, Matter Wave Lensing to Picokelvin Temperatures, Phys. Rev. Lett. **114**, 143004 (2015).

[47] C. Deppner *et al.*, Collective-Mode Enhanced Matter-Wave Optics, Phys. Rev. Lett. **127**, 100401 (2021).

[48] P. A. Altin, M. T. Johnsson, V. Negnevitsky, G. R. Dennis, R. P. Anderson, J. E. Debs, S. S. Szigeti, K. S. Hardman, S. Bennetts, G. D. McDonald, L. D. Turner, J. D. Close, and N. P. Robins, Precision atomic gravimeter based on Bragg diffraction, New J. Phys. **15**, 023009 (2013).

[49] R. H. Parker, C. Yu, B. Estey, W. Zhong, E. Huang, and H. Müller, Controlling the multiport nature of Bragg diffraction in atom interferometry, Phys. Rev. A **94**, 053618 (2016).

[50] A. Béguin, T. Rodzinka, J. Vigué, B. Allard, and A. Gauguet, Characterization of an atom interferometer in the quasi-Bragg regime, Phys. Rev. A **105**, 033302 (2022).

[51] F. Fitzek, J.-N. Siemß, S. Seckmeyer, H. Ahlers, E. M. Rasel, K. Hammerer, and N. Gaaloul, Universal atom interferometer simulation of elastic scattering processes, Sci. Rep. **10**, 22120 (2020).

[52] E. Giese, A. Roura, G. Tackmann, E. M. Rasel, and W. P. Schleich, Double Bragg diffraction: A tool for atom optics, Phys. Rev. A **88**, 053608 (2013).

[53] H. Ahlers, H. Müntinga, A. Wenzlawski, M. Krutzik, G. Tackmann, S. Abend, N. Gaaloul, E. Giese, A. Roura, R. Kuhl, C. Lämmerzahl, A. Peters, P. Windpassinger, K. Sengstock, W. P. Schleich, W. Ertmer, and E. M. Rasel, Double Bragg Interferometry, Phys. Rev. Lett. **116**, 173601 (2016).

[54] J. Jenewein, S. Hartmann, A. Roura, and E. Giese, Bragg-diffraction-induced imperfections of the signal in retroreflective atom interferometers, Phys. Rev. A **105**, 063316 (2022).

[55] P. Hamilton, M. Jaffe, J. M. Brown, L. Maisenbacher, B. Estey, and H. Müller, Atom Interferometry in an Optical Cavity, Phys. Rev. Lett. **114**, 100405 (2015).

[56] C. D. Panda, M. Tao, J. Egelhoff, M. Ceja, V. Xu, and H. Müller, Minute-scale gravimetry using a coherent atomic spatial superposition, arXiv:2210.07289.